Size effects in superfluid ^{3}He films

M. R. Freeman* and R. C. Richardson
Laboratory of Atomic and Solid State Physics, Cornell University, Ithaca, New York 14853
(Received 7 July 1989; revised manuscript received 9 January 1990)

This paper addresses two related problems. One is the effect of small geometries on the superfluid phases of ^{3}He, and the other is the nature of the scattering of ^{3}He quasiparticles at surfaces. We perform measurements on 300-nm-thick films of ^{3}He created by confining the liquid between closely spaced Mylar sheets. The fluid is probed simultaneously by two methods. Nuclear magnetic resonance monitors the spin dynamics of the system, yielding information with which we identify the superfluid phase. In this case, the liquid signal must be separated from that of the adsorbed surface layer, with which it is averaged by spin exchange. The hydrodynamic response of the fluid is determined from the period and damping of a torsion pendulum, which generates oscillatory motion of the substrate. In the normal and superfluid phases alike, this response is strongly dependent on microscopic details of the quasiparticle interactions with the surface. We compare the superfluid measurements to the Ginzburg-Landau model in which the order parameter vanishes at the walls (the diffusive boundary condition). Results for the superfluid transition temperature, the superfluid density, and the NMR frequency shift are in good quantitative agreement with the theory. Also in accord with the theory, we find that the superfluid A phase is stabilized by the walls over a wide range of pressures and temperatures at which the B phase is stable in bulk. In contrast with the calculations, however, we do not observe the A-B phase boundary. The ^{3}He-substrate interface is modified in these experiments by the introduction of small quantities of ^{4}He. ^{4}He plates out preferentially on the surfaces at low temperatures, an effect that persists until a layer several atoms deep has been built up. The boundary condition on the order parameter is observed to vary continuously with the surface ^{4}He coverage, spanning almost the full range between the limits corresponding to diffusive and specular quasiparticle scattering.

I. INTRODUCTION

In a certain sense, size effects are always present. The sample is of finite size in any real experiment and therefore has boundaries, which at some level influence the measurement. To probe true bulk properties, all of the sample dimensions must be much larger than the length scales on which the physics is determined. The results obtained are then independent of the sample size.

Examples of size effects occur most frequently in the physics of transport, for example, in the flow of a classical gas when the mean free path is larger than the diameter of the tube, or in electrical transport when the mean free path of the conduction electrons is limited by scattering at surfaces. The physical effects of interest in the present work are created by reducing the thickness dimension of ^{3}He films to the scale of the (temperature-dependent) correlation length of the superfluid phase, which is the distance over which substantial variations can occur in the order parameter characterizing the macroscopic quantum condensate. We use nuclear magnetic resonance to monitor the structure of the order parameter for the confined geometry (which tells us the phase diagram).[1] Through simultaneous NMR and torsional-oscillator measurements, we examine the high sensitivity of the superfluid state to the nature of the ^{3}He quasiparticle scattering at the solid interface.[2] We tune the boundary condition by controlling the coverage of atomic layers of ^{4}He on the surface. The boundary condition can also be studied through the flow of the normal Fermi liquid near the surface.[3,4]

The superfluid state of ^{3}He is of the Bardeen-Cooper-Schreiffer (BCS) type and admits of a Ginzburg-Landau description in the transition region. Qualitatively, the effect of confining geometry is to introduce a surface free energy term, which depends on the boundary condition on the order parameter, and alters the superfluid transition temperature and the amplitude of the order parameter. This is analogous to the situation for any other continuous phase transition, for example, the size dependence of the Curie point in thin ferromagnetic films.

For an s-wave BCS state, the Ginzburg-Landau free energy difference between the superfluid phase and the normal phase is written[5]

$$\mathcal{F}=-\alpha|A|^2+\beta|A|^4+K|\nabla A|^2 , \quad (1)$$

where A (a complex scalar) is a representation of the order parameter, related to the energy gap Δ through $A=\Delta e^{i\phi}$, ϕ being the phases. α, β, and K are coefficients, and $A=\sqrt{\alpha/2\beta}$ in the absence of gradients. α is proportional to T_c-T. When there are gradients, the length scale of spatial variation of the order parameter amplitude is the temperature-dependent correlation length, $\xi(T)=\sqrt{K/\alpha}$. In ^{3}He, however, experimental results such as the nonvanishing low-temperature magnetic susceptibility and the linear splitting of the A transition in a magnetic field,[6] point to a spin triplet, and hence odd angular momentum, order parameter. In addition to changes of the transition temperature and the amplitude of the order parameter, the consequences of confined

geometry may include the stabilization of states not found in the bulk. For Cooper pairing in a relative p wave, A is a complex 3×3 matrix and the free energy becomes (in zero magnetic field)[7]

$$\mathcal{F}=\alpha\,\mathrm{Tr}AA^\dagger+\beta_1|\mathrm{Tr}A\tilde{A}|^2+\beta_2(\mathrm{Tr}AA^\dagger)^2+\beta_3\mathrm{Tr}(A\tilde{A})(A\tilde{A})^*+\beta_4\mathrm{Tr}(AA^\dagger AA^\dagger)+\beta_5\mathrm{Tr}(AA^\dagger)(AA^\dagger)^*+\mathcal{F}_{\mathrm{grad}}\ . \tag{2}$$

$\tilde{A}$ denotes the transpose, and $A^\dagger$ the Hermitian conjugate, of A. In the so-called "weak-coupling" limit the coefficients are

$$\alpha=\frac{N(0)}{3}\left[1-\frac{T}{T_c}\right], \tag{3}$$

and $\beta_i=\beta_{\mathrm{BCS}}\tilde{\beta}_i$, where $\tilde{\beta}_i=(-1,2,2,2,-2)$ and

$$\beta_{\mathrm{BCS}}=\frac{7\zeta(3)}{240}N(0)\left[\frac{1}{\pi k_B T_c}\right]^2. \tag{4}$$

In the jargon of superfluid ^{3}He, "strong coupling" refers to the changes in the pairing interaction resulting from the formation of the condensate. This is an important effect,[8] more so than in the case of electronic superconductivity because there is no separate lattice with which the ^{3}He quasiparticles interact. Strong-coupling effects are included as corrections, $\Delta\beta_i$, to the β_i.

The problem of minimizing the free energy for arbitrary β_i is intractable. Fortunately, experimental information can be used to constrain the choices for A. For example,[9] $AA^\dagger$ is real and symmetric because there is no spontaneous magnetization. The order parameter is often represented as a 2×2 matrix in spin space,[7]

$$\Delta_{\mu\nu}\sim i\left[\left[\sum_{ij}\sigma_i A_{ij}\hat{k}_j\right]\sigma_y\right]_{\mu\nu},$$

where the σ's are Pauli spin matrices and $\hat{k}_j$ is a component of the unit wave vector $\hat{k}$. The energy gap is $\mathrm{Tr}\Delta^\dagger\Delta$. The minimization is easy when the matrix $\Delta_{\mu\nu}$ is unitary.[10] This is true of the two bulk phases, stable in zero magnetic field, A and B. The B phase is isotropic, and can be represented by

$$A_B=\frac{1}{\sqrt{3}}\begin{bmatrix}1&0&0\\0&1&0\\0&0&1\end{bmatrix}. \tag{5}$$

The A-phase energy gap has two point nodes in k space. It's order parameter is determined by

$$A_A=\frac{1}{\sqrt{2}}\begin{bmatrix}1&i&0\\0&0&0\\0&0&0\end{bmatrix}. \tag{6}$$

There exist two other phases with unitary order parameters,[10] known as the planar and polar phases. These phases may be stabilized in confined geometries, as we shall now discuss.

Spatial variations of the order parameter and the boundary conditions at smooth and rough surfaces were considered by Ambegaokar, de Gennes, and Rainer[11] (AGR). The dominant terms of the gradient free energy are quadratic in the gradients, and AGR write

$$\mathcal{F}_{\mathrm{grad}}=\sum_p\{\mathbf{K}_L|\nabla\cdot\mathbf{A}_p|^2+\mathbf{K}_T|\nabla\times\mathbf{A}_p|^2\}\ , \tag{7}$$

where the vector $\mathbf{A}_p$ has components A_{pi}. Longitudinal and transverse gradients of the order parameter are governed by different lengths,

$$\xi_L^2=\sqrt{K_L/\alpha}=\tfrac{9}{5}\xi_s^2\Big/\left[1-\frac{T}{T_c}\right] \tag{8}$$

and

$$\xi_T^2=\sqrt{K_T/\alpha}=\tfrac{3}{5}\xi_s^2\Big/\left[1-\frac{T}{T_c}\right], \tag{9}$$

where ξ_s is the low-temperature correlation length in the s-wave BCS case,

$$\xi_s=\sqrt{7\zeta(3)/48}\,\frac{\hbar v_F}{\pi k_B T_c}\ . \tag{10}$$

At an arbitrary boundary the order parameter may not easily separate into longitudinal and transverse components, and the shortest correlation length is alone often referred to[12] as

$$\xi(T)=\xi(0)/\sqrt{1-T/T_c}$$

[where $\xi(0)=\sqrt{3/5}\xi_s$]. Table I is $\xi(0)$ computed using the thermodynamic parameters of Ref. 13.

To discuss the boundary conditions, AGR consider a semi-infinite volume of ^{3}He, bounded by the xy plane. At T_c, the A matrix is linear in z,

$$A_{pi}=\mathrm{const}(b_i+z)\ . \tag{11}$$

If quasiparticles scatter specularly from the surface, AGR find that

$$A_{px}=A_{py}=\mathrm{const};\quad A_{pz}=\mathrm{const}\times z\ . \tag{12}$$

That is, the transverse components of the order parameter are unchanged, but the perpendicular component *vanishes* at the wall. This behavior is illustrated schematically in Fig. 1. AGR find for diffusely scattering surfaces a reduction of the tangential components by a factor $\xi_s/\xi(T)$, with the normal component again vanishing. In the vicinity of the transition, then, the order parameter is effectively zero at the wall, while at lower temperatures the transverse components have a finite amplitude at the boundary. The rough surface can be thought of as a plane of elastically scattering impurities, which are pair breakers in anisotropic superfluids (Anderson's theorem[14]

TABLE I. The Ginzburg-Landau correlation length coefficient, $\xi(0)$.

Pressure (bars)	$\xi(0)$ (nm)
0	50.1
3	32.8
6	25.1
9	20.7
12	18.0
15	16.0
18	14.4
21	13.3
24	12.3
27	11.5
30	10.9

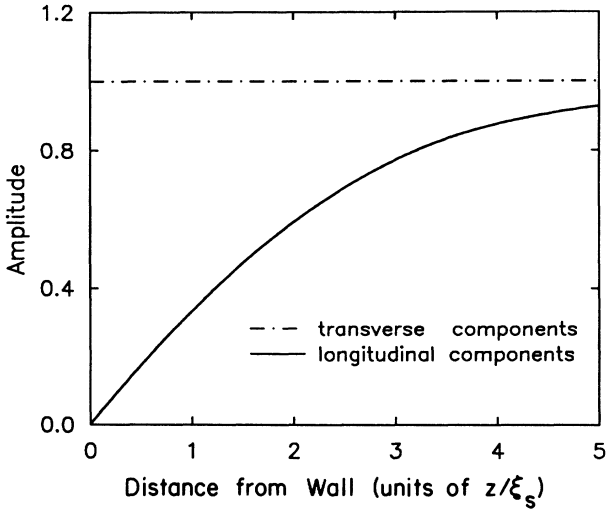

FIG. 1. The spatial variation of the amplitudes of components of the order parameter near a specular wall, at a temperature not far below T_c.

does not hold).

One immediate consequence of these boundary conditions is that the B phase is unstable in any geometry having a dimension comparable to the correlation length. Qualitatively, the quenching of the longitudinal component in films leads to the planar phase, characterized by

$$A_{\text{planar}}=\frac{1}{\sqrt{2}}\begin{bmatrix}1&0&0\\0&1&0\\0&0&0\end{bmatrix}. \tag{13}$$

In a long, narrow tube only the component along the axis survives, and one expects the polar phase,

$$A_{\text{polar}}=\begin{bmatrix}1&0&0\\0&0&0\\0&0&0\end{bmatrix}. \tag{14}$$

These qualitative statements are based on calculations which have been carried out by a number of authors. Barton and Moore predict the stability of two additional phases for the cylindrical pore in the size regime intermediate between the polar and B phases.[15] Relevant to the film geometry, Privorotskii observes that walls stabilize the A phase in the vicinity of the polycritical point, in analogy to Wheatley's "profound" effect of a magnetic field.[16] His analysis has been extended by Kuroda and Nagi[17] and by Fujita *et al.*[18] The latter authors adopt trial functions for the order parameter and perform a variational calculation to minimize the free energy. Their trial functions for the B phase are planarlike at the walls (the transverse components are in fact slightly *enhanced* near a specular surface). A transition from the A phase to a distorted B phase is predicted at a film thickness of between 7 and 15 correlation lengths, depending upon the strong coupling corrections. (Note that the definition of the correlation length above is $\sqrt{2}$ smaller than that of Ref. 18, and $\sqrt{15}$ larger than Ref. 19.) Strong-coupling corrections favor the A phase. In the weak-coupling limit, thought to be appropriate to ^{3}He at zero bars, there is no transition, just a continuous distortion of the B phase into the planar state with decreasing thickness.

More recently, variational calculations by Fetter and Ullah[20] and by Li and Ho[21] have further explored the phase diagram and responses of the order parameter (the superfluid density, critical current, and NMR behavior). Thuneburg,[22] in analogy to his studies of vortex core structures,[23] has examined surfaces states of ^{3}He B using Ginzburg-Landau theory and the specular boundary condition. He finds a surface A phase which seems to be a strong-coupling effect, in addition to the planar phase. Zhang *et al.*[24] have extended this work beyond the Ginzburg-Landau regime with the quasiclassical theory of ^{3}He and a model for surface roughness. This is an important direction for the theory as it provides predictions for the full temperature range, but they do not include strong-coupling effects. Similar work, but with a different model for the diffuse scattering, has been done by Buchholtz.[25]

A quasiclassical calculation of the B-planar transition in a film with specular surfaces by Hara and Nagai[26] suggests that extrapolations of the Ginzburg-Landau results are quite reliable provided one uses the correct temperature dependence of the energy gap. Such extrapolations are unlikely to work as well for rough surfaces, however, because of the temperature dependence of the boundary condition on the transverse components of the order parameter.

The boundary condition at specular surfaces requires a certain form of the order parameter but does not diminish its amplitude. Consequently there is no change of the transition temperature. The diminution of the transverse components at diffusely scattering walls leads to a reduction of the transition temperature in confined geometries. A numerical calculation of this, based on the AGR theory, has been performed by Kjäldman, Kurkijärvi, and Rainer[19] for the cylindrical and thin film geometries. In the limit of small suppressions (sizes greater than, say, eight zero-temperature correlation lengths, so that the transition is close to the bulk T_c), they recover the Ginzburg-Landau results. For the films, that is

$$\frac{T_c^{\text{film}}}{T_c}=\exp\left[\frac{\pi^2\xi^2(0)}{d^2}\right] \tag{15}$$

$$\approx 1-\frac{\pi^2\xi^2(0)}{d^2}. \tag{16}$$

This underestimates the transition temperature by about 25% at $d=3\xi(0)$. The complete solution reveals a critical size, $d_c=2.0\xi(0)$, below which no superfluidity occurs [to convert to the notation of KKR, $\xi_0=\xi(0)\sqrt{20/7\zeta(3)}$].

The Ginzburg-Landau result for the change in transition temperature was first obtained for superfluid ^{4}He films by Ginzburg and Pitaevskii in 1958.[27] Kiknadze and Mamaladze[28] have extended the Ginzburg-Pitaevskii analysis to calculate another major experimental quantity, the spatial average of the superfluid density. They find [for $(1-T/T_{c,\text{bulk}})\ll 1$]

$$\langle\rho_s\rangle=\tfrac{2}{3}\rho_{s,\text{bulk}}\left[1-\frac{\pi^2\xi^2}{d^2}\right]. \tag{17}$$

Similar behavior is found for the superfluid density and the NMR frequency shift in superfluid ^{3}He. This is discussed further in Sec. III, with regard to experimental results.

We summarize some of the interesting features anticipated by the theory in the phase diagram of Fig. 2. The dots indicate the normal-superfluid and A-B transition lines for the bulk liquid. In a 250-nm film with diffuse surfaces, these become the solid lines. The transition temperature is reduced, but the domain of the A phase is vastly increased. The order parameter is of course distorted from the bulk A and B forms in this case. As shown in Ref. 21, when the walls are made specular, the transition temperature recovers and the A phase encroaches a little on the B. Diffuse surfaces help to stabilize the B phase. This is because one component of the B-phase order parameter must be suppressed at the wall in any case, and the diffuse boundary condition already requires this.

As for the context of other experimental work into which this study fits, it is true that the word "confined" applies in one sense or another to every superfluid ^{3}He experiment, as wall effects typically propagate macroscopic distances into the fluid. To reiterate, our interest here is on size effects in which spatial variation of the *amplitude* of the order parameter is important. This, too, applies in every experiment sufficiently close to T_c, but typical temperature control and sensitivity levels require some dimension to be micrometer-sized or smaller. The focus of many early experiments in micron-scale geometries was on control of the "texture," or *orientation* of the order parameter. More recently, Ginzburg-Landau behavior at diffusely scattering walls has been indicated by measurements of the transition temperature and critical current in narrow channels[29–31] and in saturated films,[32–34] and by the superfluid density in porous materials.[35,36] The present work is the first case in which the superfluid response to a specularly scattering surface has been observed.

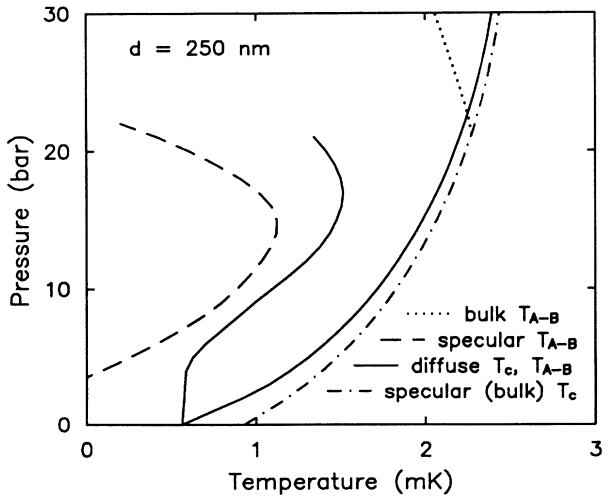

FIG. 2. A schematic phase diagram for the thin film geometry, showing the anticipated effects of both specular and diffuse surfaces. The thin film A-B phase boundaries are after Ref. 21. A region of two-dimensional superfluidity [characterized by $\xi(T) > d$] is possible close to the bulk transition line

The measurements of Manninen and Pekola[29] and of Pekola *et al.*[31] of flow through etched particles tracks in polycarbonate paper find reasonable quantitative agreement with the Ginzburg-Landau prediction for the suppression of T_c, although the data of Ref. 29 are sparse in the vicinity of the transition. The flow in these experiments was generated by diaphragm displacement. Using the torsional-oscillator technique, Kotsubo *et al.*[30] probed pores of roughly half the diameter ($\sim$350 nm). They found T_c's higher than expected. In all of these experiments, the critical currents are smaller than expected due to pair breaking, suggesting that additional mechanisms, such as vortex depinning, are at work.

One of the most appealing ways of probing the superfluid in restricted geometry is by film flow. The thickness of the film is adjustable through the height above a bulk meniscus. The greatest difficulty is in knowing the actual thickness in the presence of surface roughness. Davis *et al.*[33] decline to make an absolute estimate, whereas Daunt *et al.*[32] make a concerted effort based on Atkin's oscillations of ^{4}He. The latter authors measure T_c's consistent with Ref. 30. Very recently, however, they have found that *smoother* surfaces than those employed in Ref. 32 produce *greater* suppressions.[34] This suggests that the earlier films were thicker than previously believed.

There are always uncertainties surrounding geometric characterization in these experiments. In fourth-sound[35] and torsional-oscillator[36] measurements of the superfluid density in packed powders, no reduction of T_c is observed on account of the distribution in pore sizes. A pore-size distribution may be incorporated into the analysis of the data,[35] but this introduces many unwanted degrees of freedom. It is also difficult to assess effects of the connectivity of the pores and of the proximity effect, particularly in the transition region. The data of Ref. 35 seem to be consistent with an extrapolation of Ginzburg-Landau behavior to low temperatures, however.

The properties which we have been discussing—superfluid density, critical temperature, and critical current—are more dependent on the amplitude of the order parameter than on its structure. NMR is the most valuable experimental probe for determining the superfluid phase. The above discussion neglects the two elements crucial in determining the NMR response of superfluid ^{3}He—the nuclear dipole interaction, and the applied magnetic field. The surprising transverse NMR frequency shift of superfluid ^{3}He was elucidated by Leggett.[37] He found each unitary phase to have a characteristic NMR "fingerprint." The NMR behavior is anisotropic, however, and in a confined geometry it is important that most of the surfaces be similarly oriented with respect to the magnetic field in order to obtain meaningful results. The parallel plate and straight cylinder geometries are therefore best suited to this type of experiment. In packed powders the signal actually washes out, a problem which is more apparent at low fields, where the relative transverse shift is much larger.[38]

II. EXPERIMENTAL DETAILS

These experiments are performed on a copper nuclear demagnetization cryostat, described in detail elsewhere,[4] with a bottom temperature below 300 μK and a residual heat leak of less than 1 nW. We measure superfluid density and NMR frequency shifts simultaneously with the cell illustrated in Fig. 3. The heart of the cell is the stack of Mylar sheets which creates the helium films by confinement. To optimize the helium fill fraction we use Mylar 6C, which at 1.5 μm is the thinnest currently available.[39] The Mylar surfaces are sparsely populated with 0.5-μm diameter polystyrene microspheres[40] to establish the spacing.

The beads are deposited on the surface by misting a suspension of spheres in isopropanol onto the Mylar and allowing the alcohol to evaporate. Methanol does not seem to wet the surface, and upon drying leaves patterns of beads reminiscent of stone circles. The misting operation is done in a dust-free area, and the Mylar surface is itself sufficiently flat and clean that the polystyrene particles determine the spacing. In a similar cell for studies of ^{4}He superfluid films, Adams and Glaberson[41] stacked up Mylar sheets directly and found an open volume corresponding to an average sheet separation of 120 nm. The choice of surface density for these particles is based on a trade-off between (i) maintaining a uniform sheet spacing, and (ii) preserving the superfluid order parameter structure of a geometry with closely spaced walls and no intervening beads. A razor-sharp hardened steel punch is used to cut discs from larger sheets, and a 0.5-mm hole is punched in the center of each disc to ensure thermal equilibrium within the cell. The final stack of discs is packed tightly into an epoxy capsule. All of the sheets must be firmly entrained to obtain stable operation of the torsional oscillator. The interior of the epoxy capsule is thinly coated with silicon grease in an attempt to fill any voids which may occur at the edge of the stack, and to help anchor the individual sheets. The mean sheet spacing, which we deduce from the shift in oscillator period upon filling with liquid helium, is 280±20 nm. The uncertainty arises in our determination of the moment of inertia of the empty oscillator. Presumably the spheres compress and indent the Mylar during the packing step. This primitive fabrication method works surprisingly well. It requires the Mylar surfaces to be flat and clean. Under the electron microscope, the main surface features are 100-nm-scale pimples, and occasional larger specks of dirt.

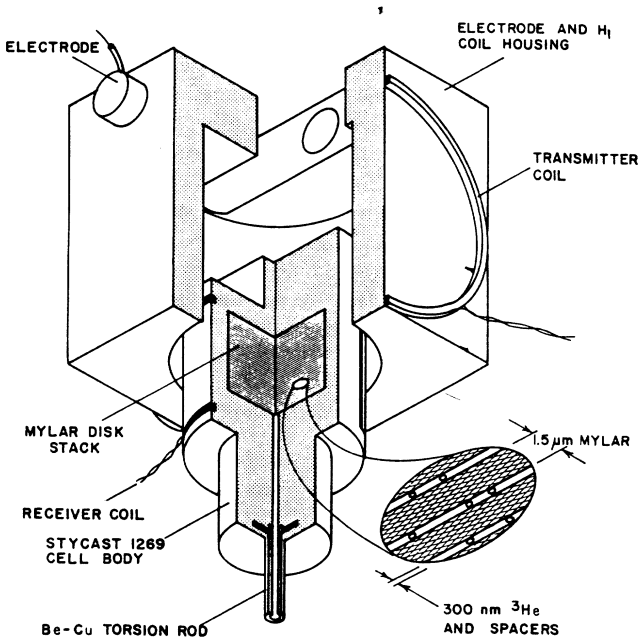

FIG. 3. The combined torsion pendulum/NMR probe. The ^{3}He in the head of the oscillator fills and cools through the hole in the torsion rod, which terminates in a small heat exchanger linked to the nuclear refrigerant. The electrode structure is thermally sunk to the mixing chamber.

Our pulsed NMR measurements are performed using a crossed-coil probe, in order to thermally anchor the transmitter coil to the mixing chamber. Since there is no physical contact between the transmitter coil form and the ^{3}He capsule, the former easily doubles as the electrode structure for an electrostatically driven torsional oscillator.[42] This structure cannot be made of metal, as is normally done, because of rf screening and eddy current heating problems. We find that an all epoxy construction, assembled with nylon screws and grease to ensure rigidity, performs adequately, with no anomalous shifts of oscillator period or dissipation. Stycast 1269A epoxy[43] is used throughout. The 1269A epoxy has less than 25% of the dielectric loss of Stycast 1266 at 1 MHz, and is in addition somewhat stronger.

As shown in Fig. 3, three no. 40 copper wires (two in a twisted pair for the NMR coil, and a third for connection to the common plate of the drive and detection capacitors) make contact to the head of the oscillator, but do not seriously degrade its performance. The torsional resonance of the pendulum is at 1750 Hz, well above the frequency of most of the (potentially parasitic) resonances of the rest of the cryostat. The torsion rod is 1.4-mm diameter beryllium-copper with a 0.9-mm diameter hole for thermal conduction through the ^{3}He.

Our thermometry is based upon the ^{3}He melting curve. We use the most recent temperature scale of Greywall.[13] Since the Greywall scale and the older temperature scale of Halperin[44] are not simply proportional at low temperatures, the Pt thermometer provides us with some means of selecting between the two. The Pt should have a strictly Curie susceptibility in this range, but when calibrated against the Halperin melting curve it appears Curie-Weiss-like, with a divergence at 250 μK. This anomaly does not arise with the new Greywall scale.[4]

We are able to measure a small thermal disequilibrium between the sample helium and the thermometers. The *bulk* ^{3}He superfluid transition is marked by a sharp increase in the dissipation of the torsion pendulum (due to the small quantities of bulk liquid present in the oscillator). As an example, when the liquid pressure is 8 bars and the oscillator is running at a typical amplitude

(chosen such that self-heating is negligible), the bulk transition in the cell occurs with the melting curve thermometer about 10 μK below the expected temperature on the Greywall scale. This temperature offset increases to only 40 μK when the "anomalous" (magnetic) Kapitza conductance channel is cut off by ^{4}He multilayers coating the sintered silver heat exchanger. In analyzing our data we always scale the temperature to the bulk transition as determined by the oscillator. (A point of notation: We use T_c exclusively to indicate bulk transition temperatures, and refer to transitions in the restricted geometry by T_c^{film}.)

A persistent-mode superconducting solenoid[45] residing in the helium bath provides the static field for nuclear magnetic resonance. The field homogeneity achieved with this arrangement is modest, about 1:10^4 for a 1-cm diameter spherical volume, limited by stray and remanent fields of the demagnetization solenoid. This enables us to measure fractional frequency shifts of 10^{-6} when the line shape remains constant. The cell and thermometers are thermally linked at the nuclear stage by half-inch thick plate. This plate is of silver for its small Schottky heat capacity in the field of the NMR solenoid. This field bathes the platinum NMR thermometer, which conveniently resonates at 280 kHz when the ^{3}He signal is at 1 MHz, and can function as a field marker as its resonant frequency is essentially temperature independent. Smaller coils inside the cryostat are used to independently vary the Pt and ^{3}He static fields as required. The large volume of the NMR solenoid necessitates a reentrant design for the tin heat switch, placing it above the mixing chamber. The performance of the apparatus is not noticeably affected by the NMR field.

The data are acquired under computer control. The magnets are left in persistent mode following a demagnetization and the temperature is stepped using pulses of heat, between each of which is allowed time for equilibration. The NMR frequencies are determined by Fourier transformation of digitized free induction decays. No corrections for decay of the magnet currents are required on the time scale of these experiments. Some heating of the cell occurs as a result of each NMR pulse. The return to equilibrium is monitored by the response of the torsional oscillator, which is very sensitive to the ^{3}He temperature below the superfluid transition. A typical thermal time constant is 5 min, limited by conduction through the fill column. We estimate the time constants for equilibration within the head of the oscillator to be much shorter.

III. EXPERIMENTS ON PURE ^{3}He

Both the NMR and torsional-oscillator results for pure ^{3}He are very well described by the Ginzburg-Landau theory, assuming diffuse boundaries. Below we explain in some detail the corrections which must be applied to the NMR data in order to separate the liquid behavior from effects of the surface monolayer of ^{3}He. This surface "solid" can be displaced by ^{4}He in order to make the NMR experiment more straightforward, which as it turns out also causes unexpected changes in the boundary condition for ^{3}He quasiparticle scattering. The results of our measurements for dilute mixtures of ^{4}He in ^{3}He are presented in the next section.

A. Pure ^{3}He NMR

Our measurements span temperatures down to $T_c/4$ at pressures between 1.5 and 22 bars, with additional observations close to the transition temperature, T_c, at 0 and 29 bars. Based on the NMR frequency shift information, we can make the following comments about the phase diagram. The A phase is stabilized by the walls over the entire phase space, even at low pressures, where the planar phase would occur if strong-coupling effects were negligible. In 280-nm films, we see a monotonic, continuous frequency shift below the normal-fluid–A-phase transition. Despite the fact that the correlation length changes by a factor of 5 when we vary the pressure, we do not observe a "B" transition (a transition to a distorted version of the bulk B phase). This is, in part, because the dimensionless thickness at which this transition takes place increases with the pressure.[20] However, our films are thicker than the critical thicknesses for formation of a B states at $T=0$ calculated by Li and Ho[21] for pressures above about 3 bars, and by Hara and Nagai[26] above 12 bars. The transition is first order, so perhaps in the experiments we supercool over it.

A lowering in temperature of the A-B phase boundary at high pressures has been observed in 4-μm thick films by Ahonen *et al.*[46] (AKP), who studied effects of superfluid confinement on the scale of the dipole bending length (typically two orders of magnitude longer than the correlation length). Two features of the AKP experiment are of particular interest here: (i) the Curie-Weiss paramagnetism of the surface layer of ^{3}He, and (ii) the NMR response of the dipole-unlocked A phase. The excess magnetization arises because surface atoms, bound by van der Waals attraction to the substrate, do not participate in the Fermi degeneracy of the liquid. This "localized" or "solid" layer has by now been studied extensively,[47] but was first demonstrated to exist by Ahonen *et al.*,[48] who found that the addition of a small quantity of ^{4}He was sufficient to make the Curie-Weiss component disappear. The NMR frequency shifts are discussed further in the following subsection.

1. Magnetization

The helium magnetization measured by pulse NMR is shown in Fig. 4 for the liquid pressure of 9 bars. We have made extensive use of these data during analysis of the frequency shifts. To illustrate the Curie-Weiss nature of the surface layer, the data are plotted as the inverse of the magnetization with the high temperature, or Fermi liquid, component subtracted off. The linear extrapolation of the high-temperature data intersects the abscissa at the Weiss temperature, $\Theta=0.5$ mK. This value is consistent with earlier measurements.[48,49] The Curie-Weiss function, $\chi=C/(T-\Theta)$, is a high-temperature approximation for systems with a ferromagnetic tendency ($\Theta>0$). The measurements deviate from this form at low

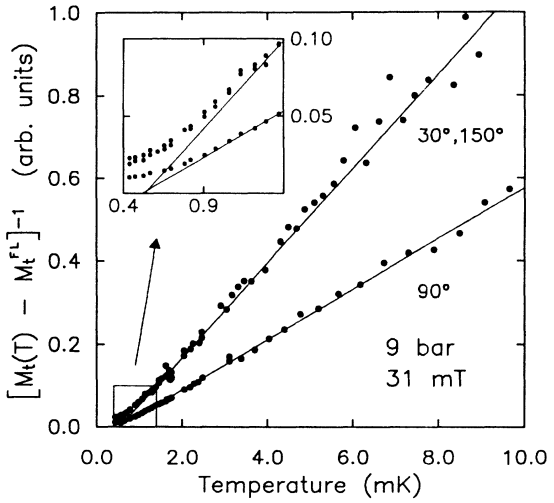

FIG. 4. The inverse localized layer transverse magnetization following a tipping pulse. The localized layer magnetization is the temperature-dependent excess above the Fermi liquid component M_t^{FL}. The solid lines are linear fits which reflect the Curie-Weiss nature of the surface layer susceptibility.

enough temperatures, as emphasized by the inset of the figure, where the polarization becomes too large for this approximation to hold. We have not endeavored to fit our data using, for example, additional terms from the expansion of the Brillouin function. Godfrin *et al.*[50] have recently analyzed the susceptibility of ^{3}He multilayers on Grafoil using ten terms of the high-temperature expansion for a 2D Heisenberg ferromagnet to describe the susceptibility of the second layer.

The spin temperature of the ^{3}He Fermi liquid at 9 bars is 256 mK.[51] Each surface atom at 1.5 mK thus contributes as much to the magnetization as 256 atoms in the liquid. Using the measured magnetization, and 8×10^{14} as the number of atoms per cm^2 on the surface, we deduce a thickness of 1.1 monolayers for the solid. This is consistent with measurements for a number of other substrates,[49,52,53] but is one order of magnitude less than the five to ten monolayers found by AKP on Mylar, and by Okuda *et al.* on silver powder.[54]

A significant feature of the magnetization data is that it shows no signature of the superfluid transition (at 1.8 mK in this case). This establishes right away that the *B* phase, with its characteristic susceptibility drop, is not present. We extrapolate the free induction decays back to the end of the rf pulses to determine the magnetization, as the NMR linewidth increases by a factor of 2 in the superfluid state. This linewidth change is larger than was found in bulk measurements by Bozler *et al.*,[55] suggesting an additional factor due to inhomogeneity in the geometry.

2. *NMR frequency shifts*

Rather than performing a continuous wave resonance experiment, it is essential to measure the resonant frequency for different pulse tipping angles in these confined geometries, in order to differentiate among sources of frequency shift which are intrinsic or external to the helium. Any tipping angle dependence of the shift represents an intrinsic effect, as the measurement is resonant and the helium spins alone are perturbed. Angle-independent effects may or may not be intrinsic. The radio frequency field is uniform over the cell, as indicated by the deep null (to less than 1% of maximum) of the signal under application of a 360° pulse. We minimize rf heating by using pulses of the longest duration, or smallest spectral width, that irradiate the frequency range of interest with adequate uniformity.

Figure 5 shows the temperature dependence of the frequency in the normal phase. The dominant behavior is pulse independent and proportional to inverse temperature. No effect of this kind is expected for helium, and we attribute it to the protons in the Mylar. The Mylar stack acts as an effective medium in which the helium is placed. It has a small volume susceptibility, κ, proportional to the number density of protons (any electronic spins are fully saturated in this regime). Mylar is a polymer of ethylene teraphthalate ($C_{10}H_{10}O_4$), for which we expect $\kappa=6\times10^{-4}/T$, where the temperature T is in milliKelvin. This compares favorably with the measured value of $4\times10^{-4}/T$ (the solid line in Fig. 5). The 90° tipping pulse result is the relevant one for comparison, as it is sensitive only to the external shifts.

The tip-angle dependence of the shift in the normal phase is an additional complication, and is due to the growing polarization of the ^{3}He surface solid. On our flat substrate this solid is a two-dimensional sheet of dipoles. A given spin in this sheet sees a field from neighboring dipoles

$$H_d=H_d^{\max}P(1-3\cos^2\phi)/2\ , \tag{18}$$

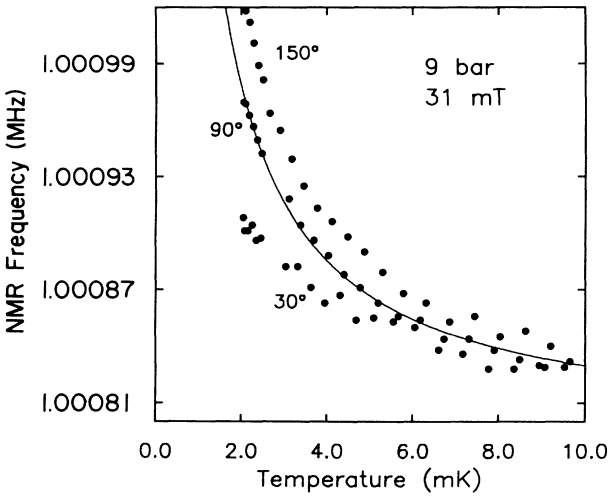

FIG. 5. The tipping-angle-dependent NMR frequency in the normal phase. The solid line shows a shift proportional to inverse temperature, which we ascribe to increasing polarization in the Mylar. The asymptotic high-temperature limit is 1.000 793 MHz.

where the angular dependence arises from the familiar anisotropy of the dipolar field.[56] $H_d^{\max}$ is the maximum dipole field, P is the polarization, and ϕ the tilt angle with respect to the surface normal of the axis along which the dipoles are polarized. In our experiment an external field $H_0 \gg H_d^{\max} P$ is applied along the surface normal, and following a ϕ degree rf pulse the spins precess in the resultant $H \approx H_0 + H_d \cos\phi$ (on time scales $\ll T_1$, which covers the entire free induction decay in this case). The observed shifts are in reasonable agreement with expectation. From the solid layer density, $H_d^{\max}$ is estimated to be 0.3 mT,[57] and the solid layer polarization at 2 mK is 1.6%. Taking into account mixing with the liquid magnetization (see below), the predicted shift at 2 mK is 45 Hz, while the measurement yields 60±10 Hz.

Although the helium polarization is large enough to produce observable frequency shifts only in the solid layer, in practice the entire signal is affected, as may be seen from the line shapes in Fig. 6. What we observe is in fact an average of the spin precession rates on the surface and in the liquid caused by rapid atomic exchange between the surface and the liquid. The spins experience both environments equally. The effect also relies on spin diffusion in the liquid sufficiently fast for uniform dissemination of information from the surface. Exorbitant exchange rates are not required in order to produce this phenomenon. If we visualize the motion in a frame rotating at one of the Larmor frequencies, it is apparent that the exchange rate need only be large on the scale of the difference frequency of the two environments. Note the qualitative difference with the original A-phase NMR experiment of Osheroff, where the spin-diffusion times across regions of bulk solid and liquid in the Pomeranchuk cell ensured the observation of a double-line spectrum.

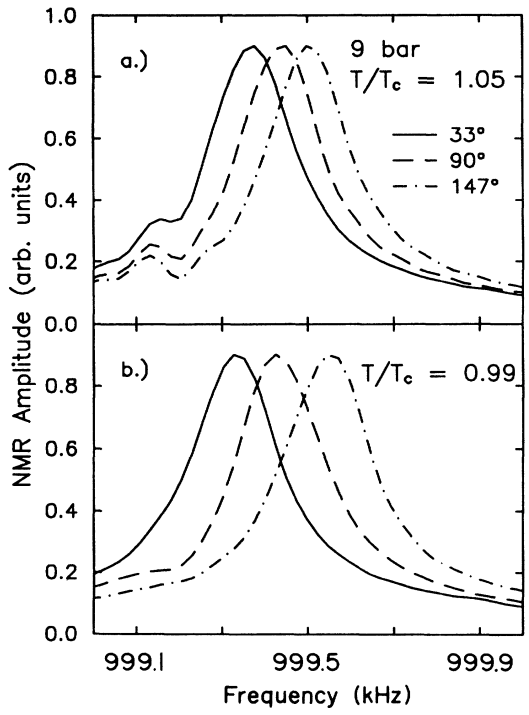

FIG. 6. ^{3}He line shapes obtained by Fourier transformation. All the heights have been normalized. The liquid magnetization is slightly greater than that of the solid under these conditions. The frequency shift causing the tipping angle dependence occurs in the surface layer, but the *entire resonance* moves due to exchange. The small side lobe is from the central column of liquid which is the main thermal artery.

This averaging is a type of motional narrowing. It is easily treated for continuous-wave NMR using the Bloch equations, as originally done by Hahn and Maxwell.[58] For the liquid-spin population we write

$$\frac{dM_t^l}{dt} = \left[-\frac{1}{T_2} + i\Delta\omega + i\frac{\delta\omega}{2} \right] M_t^l - C_l M_t^l + C_s M_t^s + i\gamma H_1 M_z^l , \tag{19}$$

where the magnetization $\mathbf{M}_l = (M_x^l, M_y^l, M_z^l)$, and we treat the transverse magnetization as the complex quantity $M_t^l = M_x^l + iM_y^l$. Referring to the liquid and solid precession rates as ω_l and ω_s, we use the notation $\delta\omega = \omega_s - \omega_l$ and $\Delta\omega = \omega - (\omega_l + \omega_s)/2$, where ω is the frequency of the H_1 field. T_2 is the transverse relaxation time of the lines (inhomogeneously broadened, in our case). C_l and C_s are transition rates for the exchange between the liquid and solid spin populations. They are related by $C_l = (M_z^s/M_z^l)C_s$, as there is no *net* transfer of magnetization between the two. A similar expression holds for M_t^s. In the steady state, the time derivatives vanish and we solve for the total transverse magnetization,

$$M_t^l + M_t^s = i\gamma H_1 \left[\frac{M_z^l \alpha_s + M_z^s \alpha_l + (M_z^l + M_z^s)(C_l + C_s)}{(\alpha_l + C_l)(\alpha_s + C_s) - C_l C_s} \right] , \tag{20}$$

where

$$\alpha_{l,s} = \frac{1}{T_2} - i\left[\Delta\omega \pm \frac{\delta\omega}{2} \right] .$$

The imaginary component of this gives the NMR absorption.

In Fig. 7 we plot the result for various exchange rates, using linewidths and relative magnetizations typical of our experiments. The double-peaked structure is eradicated when $\delta\omega/C_l \sim 1$. Only minor variations in line shape result from extending on in either direction beyond the three decades in exchange rate shown. For the largest frequency shifts which we encounter in the superfluid, exchange rates of order 10^5 sec^{-1} are sufficient to motionally average the lines. In comparison, spin transport across the films is ballistic in this regime with a characteristic time of 10^{-8} sec, and exchange rates between the liquid and the surface solid are known from longitudinal spin relaxation measurements[53] to exceed 10^8 sec^{-1}. It appears possible to design experiments which use this line-shape information to measure the exchange rate, following the lead of chemists who have studied reaction

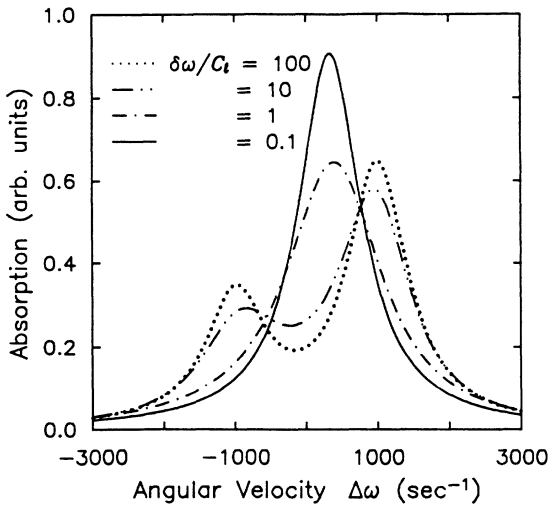

FIG. 7. The NMR absorption of two spin populations for different rates of magnetization transfer between them, as found using the Bloch equations. The frequency splitting is 2000 sec^{-1}, and the right line has twice the magnetization of the left. Both lines have $T_2=2\times10^{-3}$ sec.

rates in this manner for decades.

We attribute the small side lobe in Fig. 6(a) to the column of bulk liquid which establishes thermal equilibrium in the cell. In this case subscript l would refer to the bulk liquid in the cooling column and subscript s to the liquid in the stack. At first sight we are surprised to find two peaks, because the frequency splitting is small enough that diffusion across the column can occur in a time for which the dephasing is only one-half radian (the diffusion constant[51] is about 10 cm^2/sec). However, the bottleneck occurs for diffusion into the stack, where the thickness of the films limits the mean free path to order 1% of the bulk free path. This makes the ratio of the liquid magnetization to the surface magnetization with which it exchanges grossly larger for the bulk than for the fluid in the films. The side lobe is absorbed by the main line in the superfluid state [Fig. 6(b)], where we imagine that some faster spin transport process, perhaps a supercurrent, facilitates the averaging.

Armed with this knowledge of background shifts and exchange-averaged line shapes, we are prepared to isolated the response of the superfluid. The anisotropy of the A-phase order parameter is characterized by two unit vectors, $\mathbf{d}$ and $\mathbf{l}$, which, respectively, determine the directions of the spin quantization axis and the orbital symmetry axis of the Cooper pairs. The anisotropic terms of the free-energy density are[59]

$$F=\tfrac{1}{2}\alpha\chi(\mathbf{d}\cdot\mathbf{H})^2-\tfrac{3}{5}g_D(T)(\mathbf{d}\cdot\mathbf{l})^2+F_{\rm grad}\ , \tag{21}$$

where H is the static field, χ is the bulk susceptibility, and α is a measure of the susceptibility anisotropy. The second, or dipole, term is minimized when $\mathbf{d}$ and $\mathbf{l}$ are collinear, an arrangement which therefore obtains in sufficiently large systems. $g_D(T)$ is proportional to the square of the order parameter. At a boundary, $\mathbf{l}$ will be aligned along the surface normal.[11] In small (less than about 5 mT) magnetic fields, then, a surface also determines the orientation of $\mathbf{d}$, through the dipole energy. In larger fields the Zeeman energy dominates, and $\mathbf{d}$ lies perpendicular to $\mathbf{H}$. The gradient term establishes the length scale on which the orientation of the order parameter may vary. Here the effect of a wall on $\mathbf{l}$ propagates about 10 μm into the liquid. A uniform $\mathbf{l}$ texture is therefore found in films thinner than this "dipole-bending" length. A transverse NMR shift is caused by an additional torque of the dipole energy on the Cooper pair spins, proportional to the curvature of the dipole energy as a function of the angle between $\mathbf{d}$ and $\mathbf{l}$.[59] For films, this leads to a variation of the NMR shift from positive to negative when the field is rotated from parallel to the film (dipole-locked texture) to perpendicular (dipole-unlocked). The effect has been measured by AKP.[47] Takagi[60] was the first to predict the negative shift. Additional, interesting structure predicted for the low-field regime still awaits experimental confirmation.

The transverse resonance frequency in the superfluid A phase follows

$$\nu^2=\nu_L^2+\frac{c}{4\pi^2}\Omega^2(T)\ , \tag{22}$$

where ν_L is the unshifted Larmor frequency and $\Omega(T)$ is the (field-independent) rate of the longitudinal resonance predicted by Leggett,[61] which grows with the order parameter. The factor c is dependent both upon the texture and the tipping angle ϕ in pulse NMR. For the bulk or dipole-locked case,[62] $c=\frac{1}{4}+\frac{3}{4}\cos\phi$. The frequency shift is symmetric about $\phi=90°$ in the dipole-unlocked texture,[2] with $c=-\cos\phi$. Figure 8 shows the spin precession frequency for several tip angles as a function of in-

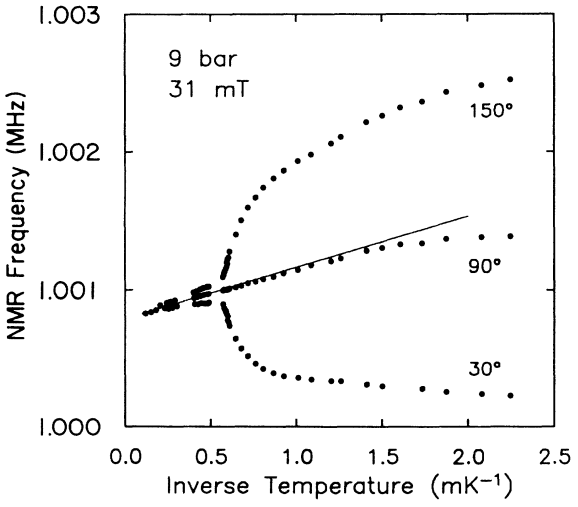

FIG. 8. The NMR frequency for several tipping angles, vs inverse temperature to emphasize the superfluid region. The line is the fit to the normal phase data from Fig. 5. The bulk transition at this pressure occurs at $T^{-1}=0.56$ mK^{-1}. The behavior is characteristic of the A phase in the dipole-unlocked texture.

verse temperature, to linearize the background shift and to emphasize the low-temperature behavior. Note that it is essential to take the background into account in order to see the symmetry about 90°. We have confirmed the cosine dependence with additional tip angles.[2]

The data of Fig. 5 occupy the region below 0.5 mK^{-1} in Fig. 8. The line accompanying the 90° data is the $1/T$ fit from the earlier figure. We attribute the deviation of the data from the line at low temperatures to thermal decoupling of the protons in the Mylar.

Eliminating the Mylar proton and solid ^{3}He layer shifts, and correcting for motional averaging, we can extract the unadulterated NMR frequency shift of the liquid in the superfluid phase. This is shown for the transition region at 9 bars in Fig. 9. We show the absolute value of the shift to emphasize the symmetry of the 30° and 150° pulse angle results. The straight line is a fit to determine the slope of the shift at the transition, which is a measure of the strength of the order parameter in films. The Ginzburg-Landau theory predicts the ratio of this slope to the same quantity for bulk. The initial slope is conventionally referred to as

$$f^2(P)=d\Omega^2/d\left[\frac{T}{T_c}\right] .$$

The Ginzburg-Landau prediction for the initial slope of the frequency shift at $T_c^{\rm film}$ for a film with rough (diffusely scattering) surfaces is simply $\frac{2}{3}f^2_{\rm bulk}(P)$. This assumes only that the temperature dependences of $\Omega^2_{\rm bulk}$ and of the correlation length ξ are, respectively, $[1-(T/T_c)]$ and $[1-(T/T_c)]^{-1/2}$. The result is independent of the actual thickness d of the film because the dimensionless thickness $w=d/\xi$ is a constant (π) at the transition. Of course, the temperature window over which w remains small shrinks into invisibility for large d. The actual expression for the NMR shift near T_c is

$$\frac{\Omega^2}{\Omega^2_{\rm bulk}}=\frac{2}{3}\left[1-\left[\frac{\pi}{w}\right]^2\right] . \tag{23}$$

For the data as plotted in Fig. 9, the slope can be written

$$\frac{d\delta\nu}{d\left[\frac{1}{T}\right]}=\frac{T_c^{\rm film}f^2_{\rm bulk}(P)\cos\phi}{3\nu_L} . \tag{24}$$

Using bulk data (see below), we find 6.9×10^3 Hz mK, in fair agreement with the fit to our data, 5.7×10^3 Hz mK.

The low-pressure half of the bulk phase diagram (where the B phase alone occurs normally) is largely unexplored as far as the A phase is concerned, although it is possible to stabilize the A phase with a magnetic field.[63] There exists one measurement for the 6-μK sliver of A phase in 28 mT at 2 bars.[64] To our knowledge this is the only data point. We use this result and the numbers for intermediate pressures obtained by interpolation. Estimates of the A-phase frequency shifts based upon the B-phase measurements[65] seem to agree rather well with the interpolation.

Figure 10 displays a comparison of experimental frequency shift slopes, $-A(P)f^2(P)$, and the Ginzburg-Landau prediction for a range of pressures. The factor $A(P)$ represents the backgrounds and effects of exchange averaging with the solid magnetization, which in this case are folded into the Ginzburg-Landau estimate (the line in the figure) rather than removed from the data. From the measurements at 9 bars, we extend the ratio of liquid and solid magnetizations to other pressures using the known pressure dependences of the liquid molar volume and magnetic Fermi temperature.[66,51] We assume that the pressure dependence of the number of atoms in

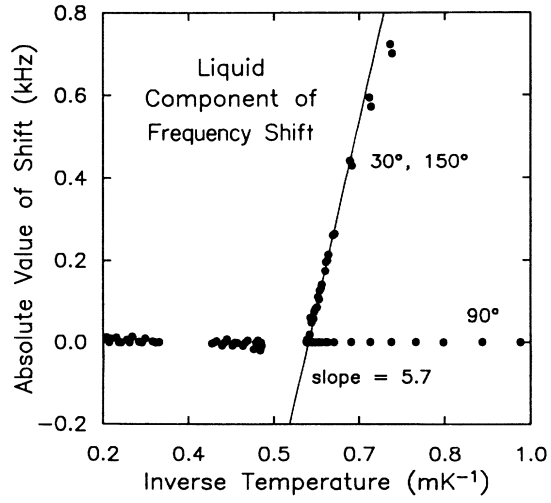

FIG. 9. The NMR frequency shift of the ^{3}He liquid, liberated from the many burdens which encumber it in the raw data.

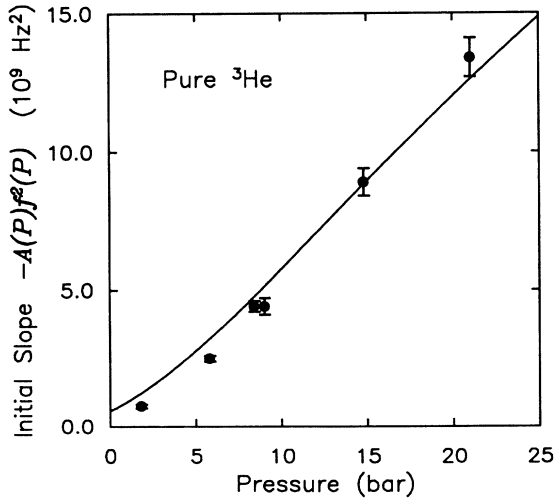

FIG. 10. The symbols are our measured initial slopes of the NMR frequency shift for pure ^{3}He at a variety of pressures, using 30° tipping pulses. The solid line represents the slopes that we expect within the Ginzburg-Landau theory, based on our knowledge of the magnetization in the system.

solid ^{3}He layer is negligible, as has been found in some other experiments.[67] There is evidence for the number of atoms in the solid ^{3}He layer increasing by 40% from 0 to 25 bars on a fluorocarbon substrate.[53] Such an effect would decrease the slope of the solid line in Fig. 10 by a small amount.

We can confirm our identification of the A phase by observing the variation of texture with field direction. We tilt the static magnetic field on the cell using large room-temperature Helmholtz coils to apply a horizontal field (this field is able to penetrate the vertical superconducting solenoids), which cannot screen fields in the horizontal plane. In Fig. 11(a) we show results for a 7.7-mT field in two different orientations. The frequency shift on cooling through the superfluid transition is actually positive with the field parallel to the films, indicating the dipole-locked texture. We plot the absolute values of the shifts to facilitate comparison of the slopes. These data are *not* corrected to isolate the liquid response. The amplitude of the dipolar frequency shift in the solid layer is smaller by a factor of 2 for the parallel field [see Eq. (18)], perhaps explaining the small discrepancy which grows with decreasing temperature.

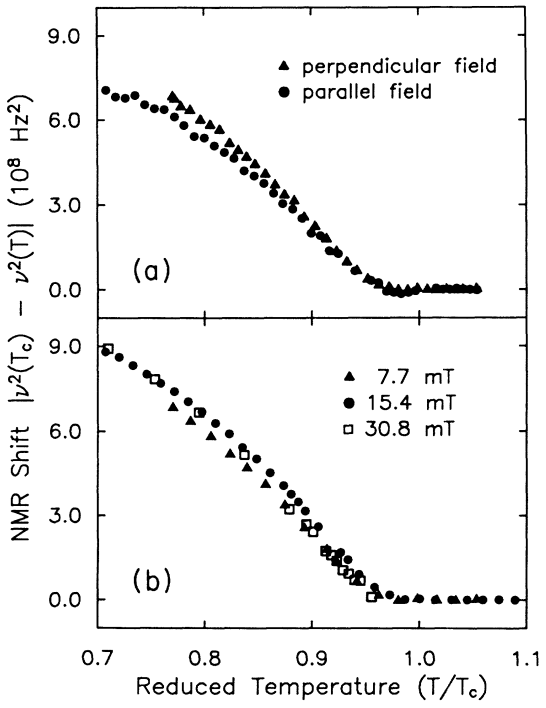

FIG. 11. The field independence of the Leggett frequency (here $\Omega^2/4\pi^2$), defined in Eq. (22). The results in (a) are measured in a 7.7-mT field at a liquid pressure of 9 bars. The field direction indicated is with respect to the plane of the films. The parallel field stabilizes the "dipole-locked" texture and changes the sign of the frequency shift. The difference which grows with decreasing temperature is an effect of the solid layer (these are raw data). Part (b) shows results for three magnitudes of the perpendicular field. The texture is field independent in this range.

Figure 11(b) displays measurements of the NMR response for three values of the perpendicular field. Each field is strong enough to establish the orientation of **d**. In this case there are small variations between the data sets which cannot be explained by the solid layer, but we are reluctant to ascribe to them any significance.

B. Pure ^{3}He superfluid density

We now move on to discuss the superfluid density ρ_s. A comparison of these measurements with the Ginzburg-Landau theory is more straightforward than is the case for the NMR experiment. As the viscous penetration depth is tremendously longer than the ^{3}He film thickness, the normal fluid is well locked to the substrate and the reduced superfluid density is related to the oscillator period $\mathcal{P}$ by

$$\frac{\rho_s}{\rho}=\frac{\mathcal{P}(T_c)-\mathcal{P}(T)}{(1-\chi)(\mathcal{P}_{\text{full}}-\mathcal{P}_{\text{empty}})}\ , \tag{25}$$

when the ^{3}He contributes only a small fraction of the total moment of inertia of the oscillator. The complete ^{3}He component of the moment of inertia is responsible for a period shift $\mathcal{P}_{\text{full}}-\mathcal{P}_{\text{empty}}$, but imperfections in the flow paths keep a fraction χ of this coupled to the oscillator when the liquid is completely superfluid. We find $\chi=0.27$ in a calibration with pure ^{4}He, which develops its bulk superfluid density in a geometry of this size. A small, helium-filled gap exists at the edge of the cell because the Mylar sheets are not perfectly flush with the epoxy wall, and the grease does not perfectly fill the voids. The average thickness of this gap is 10 μm. It corresponds to 6% of the ^{3}He moment of inertia and contributes a bulk superfluid density, which we subtract from the data. Note that the fractional effect of this helium excess on the NMR measurements is smaller by a factor of 2, because of the heavy weighting of the moment of inertia at large radii.

Our experimental determinations of ρ_s/ρ at a variety of pressures are shown as Figs. 12 and 13. In the transition region, the Ginzburg-Landau prediction for the superfluid fraction of a ^{4}He film (assuming that the order parameter vanishes at the surfaces) is[28]

$$\frac{\langle\rho_s\rangle}{\rho_{s,\text{bulk}}}=\frac{4}{3}\left[1-\frac{\pi}{w}\right]\ , \tag{26}$$

where w is again the dimensionless thickness, measured in units of the correlation length. $\langle\rho_s\rangle$ is the experimentally relevant quantity, the spatial average of the superfluid density across the width of the film. The actual superfluid transition in ^{4}He films turns out to be of the Kosterlitz-Thouless variety; however, the applicability of a healing-length picture to superfluid ^{4}He is questionable.[68] The result would apply to superfluid ^{3}He if it were isotropic. For ^{3}He A, Eq. (26) becomes[12]

$$\frac{\langle\rho_s^A\rangle}{\rho_{s,\text{bulk}}^A}=0.6209\left[1-\left[\frac{\pi}{w}\right]^2\right]\ . \tag{27}$$

This expression differs from Eq. (26) by 7% near the tran-

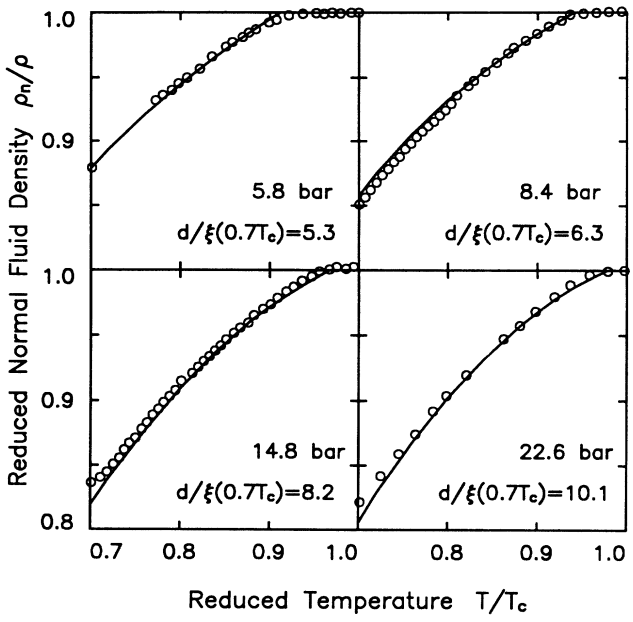

FIG. 12. The normal fluid density of pure ^{3}He as measured by the torsional oscillator. The solid lines are the Ginzburg-Landau predictions based on Cornell data for the bulk B-phase superfluid density, with *no* free parameters.

sition ($w=\pi$); the prefactor is affected by an off-diagonal component of the order parameter that becomes nonzero during flow. For large thicknesses, the superfluid fraction is determined by the proportion of liquid within a distance of order $\xi(T)$ from the wall:

$$\frac{\langle \rho_s \rangle}{\rho} = 1 - \frac{k(w)}{w} . \tag{28}$$

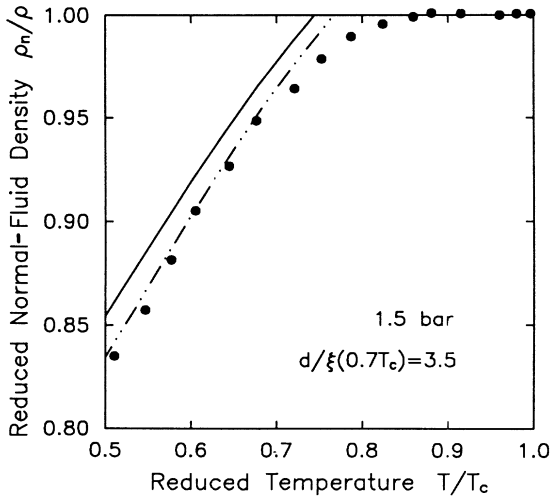

FIG. 13. A lower pressure data set. The rounding near the film transition is more apparent, as the correlation length is a less strong function of temperature in the vicinity of the transition. The solid and dash-dot-dotted Ginzburg-Landau lines take $d=280$ nm and $d=290$ nm, respectively.

When $w \gg \pi$, $k=\pi$ in the calculation for ^{4}He,[28] whereas $k=3.2$ for ^{3}He A.

We interpolate between Eqs. (27) and (28) at intermediate w in order to generate a Ginzburg-Landau prediction for comparison with our measurements. This procedure agrees well with numerical calculations.[21,69] The temperature dependence of the correlation length is normally written

$$\xi(T)=\xi(0)\left[1-\frac{T}{T_c}\right]^{-1/2} , \tag{29}$$

where

$$\xi(0)=\left[\frac{7\zeta(3)}{80}\right]^{1/2}\frac{\hbar v_F}{\pi k_B T_c} .$$

We use Greywall's recent results[13] to compute $\xi(0)$. v_F is the Fermi velocity and ζ is the Riemann zeta function. The Ginzburg-Landau description of the p-wave superfluid actually has two (longitudinal and transverse) correlation lengths.[11] Following the convention of Buchholtz and Fetter,[12] $\xi(T)$ is taken to be the shortest (transverse) one. The temperature dependence in Eq. (29) is correct only close to the transition [$\xi(0)$ is *not* the true zero temperature correlation length]. Einzel[70] gives a form, that we use, which interpolates between this Ginzburg-Landau form and the low-temperature behavior appropriate to the BCS gap. In practice it makes little difference which form is used over the temperature range of Fig. 12. A numerical calculation would be necessary to determine the correct dependence for the confined geometry at low T/T_c.

It is necessary to elaborate a bit about the bulk data with which we make our comparisons to theory. The A-phase superfluid density is anisotropic, and to our knowledge there exists only one measurement of the component, $\rho_s^{A,\perp}$ for flow perpendicular to $\boldsymbol{l}$. This was reported by Berthold *et al.*[71] for a 27-bars liquid pressure. The appropriate $\boldsymbol{l}$ texture was stabilized by a magnetic field. At other pressures we obtain the A-phase superfluid density from B-phase measurements, through $\rho_s^{A,\perp}=2\rho_s^B/5\bar{\beta}_{245}$. We use the most recent Cornell data[72] for the B-phase superfluid density, and find close agreement with the Berthold result at 27 bars. This, as well as the apparent consistency with our own results, increases our confidence in this bulk data. There is a surprising amount of variation between different measurements of ρ_s^B. These discrepancies are more serious than simple temperature scale differences, as they are apparent even at reduced temperatures close to unity.

It is evident in Fig. 13 that the experimental superfluid density does not vanish at $T_c^{\rm film}$. Thuneberg has suggested[73] that the rounding of the data could be due to a proximity effect, in which superfluidity in the films is induced by bulk liquid at the edges. Alternatively, such an effect can be due to a dispersion in the film thicknesses present in the sample. In Fig. 12 we use $d=280$ nm, a number determined from the period shift of the oscillator upon filling with helium, but therefore indicative only of the average film thickness. We plot in Fig. 14 an expanded

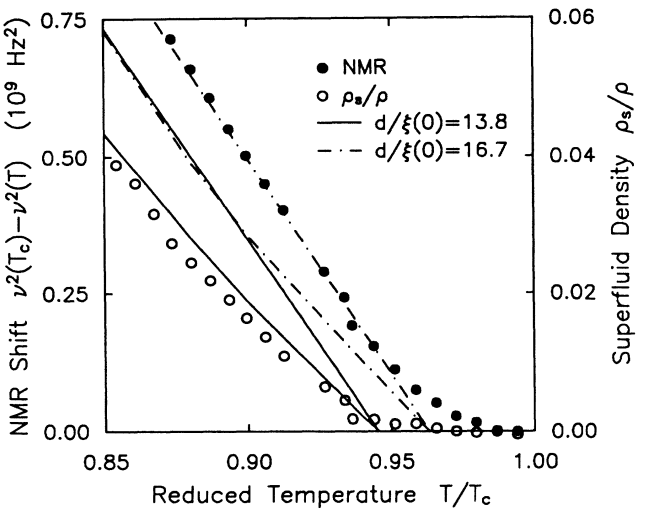

FIG. 14. Detail of the Ginzburg-Landau fits to the 8.4-bars data set. The NMR and torsional-oscillator measurements extrapolate to slightly different T_c^{film}'s, corresponding to $d=350$ nm and 290 nm, respectively. This suggests that the geometry is not perfectly characterized. The parallel, straight solid, and dash-dotted lines are the NMR predictions for the two thickness. The slightly curved lines show the expected superfluid density.

view of the transition region for the 8.4-bar data, with the simultaneously acquired NMR shift included for comparison. A common temperature scale is ensured by the nature of the experiment. The Ginzburg-Landau curves which best fit the two measurements extrapolate to slightly different film transition temperatures. The two solid lines show the expected torsional-oscillator and NMR responses for $d=300$ nm. A superior fit to the NMR data is obtained with the dash-dot lines, corresponding to $d=350$ nm. Note that these fits assume that whatever causes the rounding has no consequences at lower temperatures.

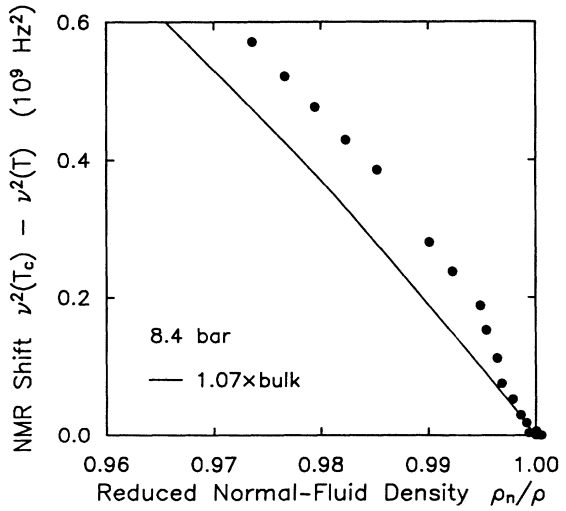

FIG. 15. The frequency shift and normal fluid density plotted one vs the other. The solid lines shows Ginzburg-Landau behavior. This result is very sensitive to the corrections required to isolate the liquid NMR signal.

It is interesting to plot the NMR frequency shift versus the normal fluid density. Inspecting Eqs. (23) and (26), we see that the result should be a straight line with slope equal to 1.07 times the slope of the same line for bulk ^{3}He *A*. In Fig. 15 the deviation of our data from this behavior is apparent. One possibility is to explain this as a consequence of the fact that the torsional-oscillator response is sensitive to how regions of superfluid are connected, while NMR is a local probe. Inhomogeneity in the sample then leads to an effective temperature dependence of the factor χ as the correlation length changes. A modeling procedure of the type used in Ref. 35 to account for a sample size distribution will always reproduce the bulk line in a $\Delta\nu^2$ versus ρ_n/ρ plot.

IV. EXPERIMENTS ON DILUTE MIXTURES OF ^{4}He IN ^{3}He: CHANGING THE BOUNDARY CONDITION

When a container is filled with a binary liquid mixture, one expects the walls to be coated preferentially by the component having a stronger attraction to the surface. In the case of isotopic mixtures of helium, the van der Waals interaction is the same for both components and it is the zero-point energy that makes the difference. By virtue of its greater mass, the zero-point motion of a ^{4}He atom is less than that of a ^{3}He atom. That is, the ^{4}He species is effectively smaller, and both covers the surface with a greater number density and sits slightly deeper in the van der Waals potential well.

The first experimental consequence of this was found by Laheurte and Keyston,[74] who observed a ^{4}He superfluid film at a temperature above phase separation for a dilute mixture of ^{4}He in ^{3}He. The surface ^{4}He film can have a large effect on the boundary condition for scattering of ^{3}He quasiparticles, which seriously complicates attempts to measure the effective viscosity of mixtures. This effect, once believed to be well characterized,[3] has recently proven to have more subtleties.[75] In addition to altering the momentum scattering, the presence of small amounts of ^{4}He in ^{3}He has an enormous influence on energy transport across boundaries. When the ^{3}He next to a surface is promoted into the liquid, the important magnetic channel coupling to spins in the solid is cut off[76] and the Curie-Weiss magnetization of the localized atoms disappears.[48] In this section we present results which demonstrate these sorts of effects in a dramatic way, exploiting the surface sensitivity of superfluid ^{3}He films. The mixtures that we deal with are sufficiently dilute that they phase separate at the surfaces, leaving most of the helium as essentially pure ^{3}He. Typically the ^{4}He is admitted to the cell before the ^{3}He, rather than together as a mixture. The surface area of the silver sinter acts as ballast which makes the total quantity of ^{4}He large enough to be easily controlled. The ^{4}He concentration profile at the surface in these systems is discussed in Ref. 77.

A. Calibration and characterization of surface ^{4}He films

The high sensitivity of the torsional-oscillator technique enables us to calibrate the ^{4}He surface coverage using the Kosterlita-Thouless transition.[78] The first monolayer of ^{4}He is densest, at about 18 μM/m^2. The density drops rapidly with distance from the surface, to about 13 μM/m^2 for liquid layers at saturated vapor pressure. An inert layer of 28 μM/m^2 must be completed before any superfluid appears. The Kosterlitz-Thouless transition temperature arises, linearly at first, with additional coverage beyond this critical value. A typical transition in this cell is shown in Fig. 16.

We introduce the ^{4}He into the empty cell at 8 K in an effort to obtain uniform submonolayer coverages. Our refrigerator is relatively slow to start from this temperature, giving the film a few hours to anneal. The anneal was unsuccessful for our first dose. We admitted enough atoms to complete a monolayer, but achieved a coverage on the Mylar of only one-quarter monolayer. We are able to measure submonolayer coverages using either the low-temperature magnetization or the spin-lattice relaxation time T_1 of the ^{3}He. T_1 is surface dominated[79] and is increased a factor of 50 by multilayer ^{4}He coverages in our experiment. Our pure ^{3}He T_1 is 30 msec at 5 mK in a field of 31 mT, closely agreeing with the results of Hammel.[49] The T_1 increases by a factor of 3 with one-quarter monolayer of ^{4}He, while the Curie-Weiss component of the magnetization decreases by 25% relative to the pure ^{3}He value. This low coverage of ^{4}He has no discernible effect on the superfluid density. We have not examined other submonolayer coatings.

32 μM/m^2 is a special coverage (seen later in Fig. 20) because it is approximately the thickest ^{4}He layer that we can use while remaining sure that there is no *superfluid* ^{4}He under the ^{3}He. This threshold was found by McQueeney, Agnolet, and Reppy[80] in studies of the effect of ^{3}He coverage on the Kosterlitz-Thouless transition in ^{4}He films on Mylar. For bare ^{4}He films with Kosterlitz-Thouless transitions at 500 mK or less, they found that the addition of only a couple of monolayers of ^{3}He seems to suppress the transition to zero temperature. The transition of our bare 32-μM/m^2 film is at 300 mK, and we confirm the result of Ref. 80 by observing a suppression of the transition to 200 mK by an 18-μM dose of ^{3}He. Our quoted coverage is based on the data of Agnolet[81] for a Kosterlitz-Thouleess transition at the same temperature. Agnolet's substrate was also Mylar, and the temperature is low enough that vapor pressure effects are negligible (important because the result is then independent of the ratio of surface area to open volume in the cell). We can estimate the total surface area in the cell from the metered quantities of helium. The ^{4}He dose leading to the Kosterlitz-Thouless transition yields 8 m^2, while the ^{3}He dose produces 7 m^2. These numbers roughly correspond to a silver sinter surface area of 2 m^2/g, in good agreement with most Brunauer-Emmett-Teller measurements of other groups. The geometric surface area of the Mylar in our cell, 0.2 m^2, is only a small fraction of this total area, so our coverage determination rests on the assumption that the helium films coat Mylar and sintered silver to the same thickness.

At ^{4}He coverages high enough to exhibit superfluidity even when submerged by ^{3}He, we find some drift of the ^{4}He transition temperature with time (on the scale of days). This is probably due to ^{4}He going into solution in the warmer sections of the fill capillary. Future work of this type would best be performed with a valve on the mixing chamber.

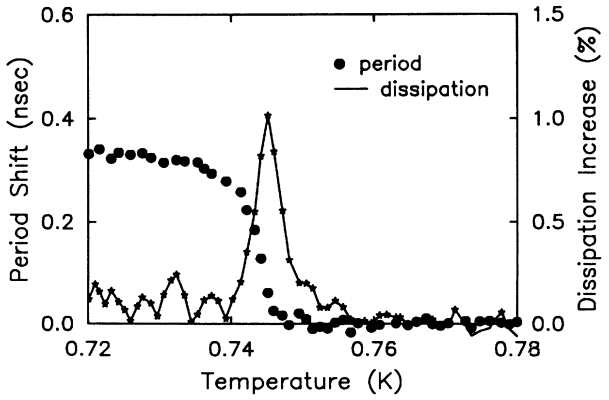

FIG. 16. The signature of the Kosterlitz-Thouless transition in a ^{4}He film in this cell. The transition temperature is used to calibrate the ^{4}He coverage, using the results of Ref. 34.

B. NMR results with surface ^{4}He

In Fig. 17 we show the low-temperature magnetization and the normal phase NMR frequency of a ^{3}He sample separated from the Mylar surface by a lining of 70 μM/m^2 of ^{4}He. The magnetization of the lowest temperature data point shown in Fig. 17(a) is one-quarter of the pure ^{3}He value, indicating the high degree of accuracy to which the Curie-Weiss component has been removed. Frequency shifts in the normal phase are also gone [Fig. 17(b)], including the background shift caused by the proton polarization in the Mylar. The protons thermally decouple at some higher temperature because of the vast increase in spin-lattice relaxation time caused by the ^{4}He buffer layer.[79] The tipping-angle-dependent shift of Fig. 5 of course, goes the way of the Curie-Weiss magnetization.

Some normal phase line shapes for the 70-μM/m^2 surface ^{4}He sample are displayed in Fig. 18. The side-lobe left behind by the growing Mylar polarization is gone (compare Fig. 6, but be aware that the static field is not exactly the same for both). We have not traced the origin of the slight skew of the line at large tipping angles. Spin waves would appear on opposite sides of the line for pulses on opposite sides of 90°.[82] In the superfluid phase we have clearer evidence for spin waves at large tipping angles.[4] We have not pursued this issue by varying the field gradient.

Raw NMR frequency shifts from the Larmor resonance at 1 MHz are plotted in Fig. 19. The liquid behavior is dramatically resolved by the addition of ^{4}He, indicated by the solid symbols in the figure. In pure ^{3}He, the

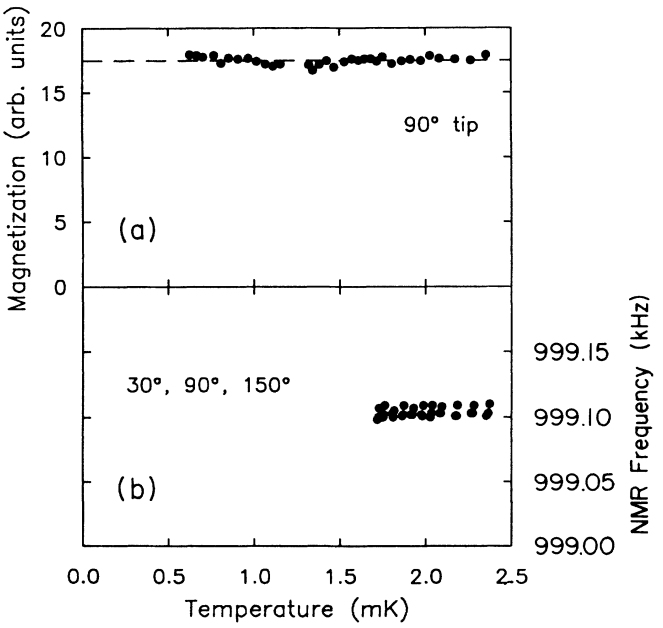

FIG. 17. The NMR response of the ^{3}He sample with a 70-μM/m^2 coverage of ^{4}He on the Mylar surfaces. This is a 9-bar data set, and the superfluid transition is at 1.7 mK. The Curie-Weiss component of the magnetization has been eliminated by the ^{4}He, and there is no longer a significant frequency shift in the normal phase (compare Figs. 4 and 5).

background effects are so large at low temperatures and low pressures that there is no sharp indication of the superfluid transition in the NMR data.

It is very interesting to compare these dilute mixture NMR shifts with the liquid behavior which we determined from the pure ^{3}He data. Some results at 8.5 bars

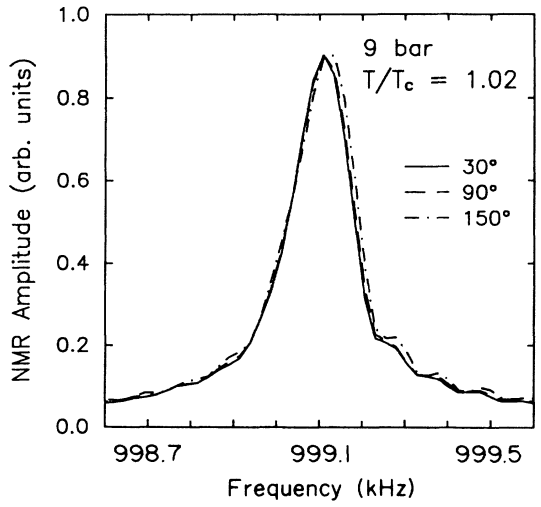

FIG. 18. Normal phase line shapes with ^{4}He coated surfaces. The tipping-angle dependence is negligible.

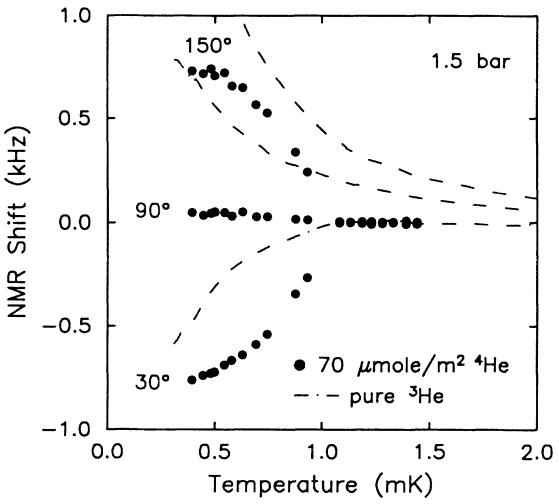

FIG. 19. ^{4}He surface coverage dependence of the raw NMR shift for different tipping angles. The Larmor resonance is at 1 MHz.

are shown in Fig. 20. The 0-μM/m^2 (i.e., pure ^{3}He) data have been purged of nonliquid effects. We are surprised to discover that removal of the Curie-Weiss magnetization is not the only consequence of ^{4}He preplating. In addition, the superfluid order parameter is substantially enhanced, as though the surfaces become more specular for scattering of ^{3}He quasiparticles. This phenomenon, first seen through its effect on measurements of the viscosity of dilute mixtures, is vividly manifest here as a reduction of the pair-breaking efficiency of the wall. The

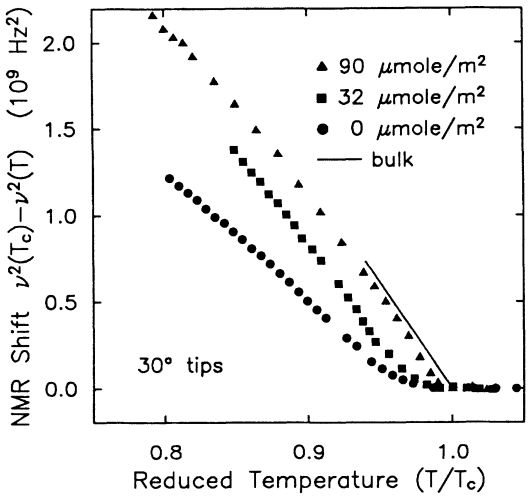

FIG. 20. The NMR shift for the three different boundary conditions, corresponding to 0-, 32-, and 90-μM/m^2 ^{4}He coverages. The ^{3}He pressure is 8.5 bars. The ordinate represents the squared Leggett frequency, in the measurement spatially averaged across the width of the film.

90-μM/m^2 ^{4}He coated surface is almost fully specular, as judged by comparison with the bulk NMR frequency shift.

It is clear from Fig. 20 that two monolayers of surface ^{4}He (with no superfluid component) have a large effect on the boundary condition for ^{3}He quasiparticle scattering. What is *not* clear is how to describe this effect, even within the phenomenological context of Ginzburg-Landau (GL) theory. We do not expect any temperature dependence of the boundary condition at these low temperatures ($T \ll T_F$). The superfluid density has not yet been calculated using the numerical models which allow the surface roughness to vary.[24,25] In the GL model we have one free parameter, the dimensionless thickness. Qualitatively, the spatial average of the order parameter in a film with partly specular walls is like that of a thicker, completely diffuse walled film. Figure 21 is a blowup of Fig. 20, showing linear fits to the data as solid lines and the Ginzburg-Landau results for three different film thicknesses as dotted lines. From left to right, the dotted lines correspond $d = 350$, 470, and 2500 nm. The 90-μM/m^2 surface is indeed highly specular, responding like a diffuse walled film an order of magnitude thicker than it actually is. The 32-μM/m^2 data do not conform to *any* single effective thickness. The slope of its linear fit is close to the bulk slope, while the intercept is at the film transition temperature for $d = 390$ nm.

C. Superfluid density with surface ^{4}He

The superfluid density reflects the same behavior as a function of ^{4}He coverage, as can be seen in Fig. 22. The 32-μM/m^2 data do not deviate as rapidly from the Ginzburg-Landau line in this case, however. We demonstrate this more clearly in Fig. 23, a plot, like Fig. 15, of the NMR response versus that of the torsional oscillator.

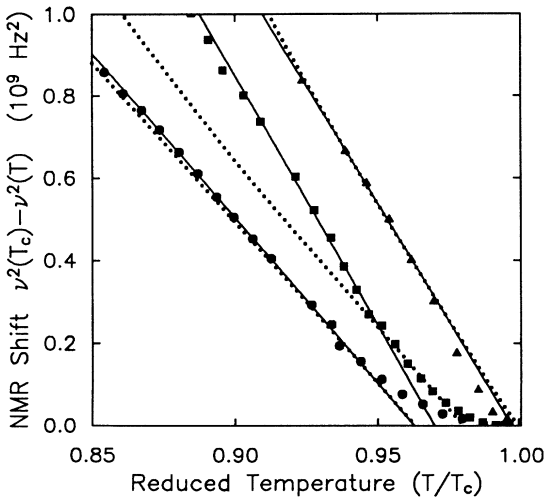

FIG. 21. A blowup of Fig. 20, with linear fits to the data shown as solid lines, and dotted lines indicating the Ginzburg-Landau result for, from left to right, $d = 350$, 470, and 2500 nm.

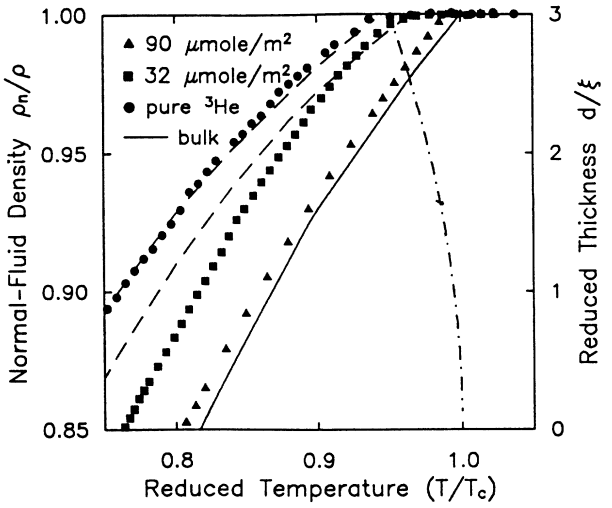

FIG. 22. The ^{3}He normal fluid density at 8.5 bars, for three different surface coverages of ^{4}He. The two dashed lines are the Ginzburg-Landau results for $d = 290$ and 360 nm. The dot-dashed line indicates the temperature variation of the dimensionless thickness. Here we have broken the $w = \pi$, but now the $w = 1$, barrier.

The 32-μM/m^2 data surprisingly deviate even more from the expected GL behavior than the pure ^{3}He data. This is, apparently, at odds with an explanation of the deviation in terms of a temperature-dependent χ factor due to the changing correlation length. Within that picture, the discrepancies should decrease as the interval of suppressed transition temperatures converges, with increasing specularity, on T_c, a trend which is recovered as the ^{4}He coverage increases (indicated by the 90-μM/m^2 data).

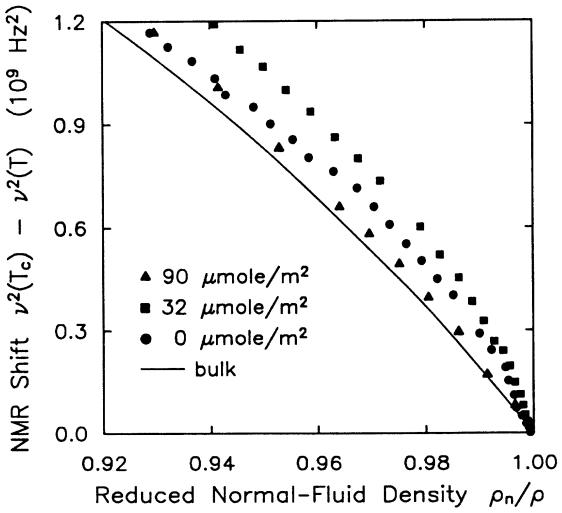

FIG. 23. The NMR and torsional-oscillator responses from Figs. 20 and 22, plotted one vs the other as in Fig. 15. The 32-μM/m^2 data show a surprising increased deviation from the bulk behavior.

D. Discussion of the boundary condition

What is the nature of the mechanism causing pair breaking at the surface, and how is it affected by ^{4}He coverage? The Ginzburg-Landau model treats the order parameter reduction at the wall phenomenologically. It does not specify a mechanism by which that boundary condition is established. It is a fragile characteristic of anisotropic superfluids that this can be done by elastic scattering. The standard assumption for ^{3}He is that the pair breaking is due to elastic quasiparticle scattering from geometrical surface roughness—a reasonable assumption, as no experiments have yet been performed on carefully prepared surfaces of known morphology. Roughness on the scale of the quasiparticle wavelength (1 nm) dominates; variations on longer length scales are less efficient at depairing.[25] The correlation length is not special in this regard. The superfluid state is constructed in a self-consistent manner which takes into account how quasiparticles scatter from the wall.

It is suggestive that the thicknesses of the ^{4}He films which we put down are comparable to the quasiparticle wavelength, and might therefore smooth out roughness on the appropriate scale, especially in the case of multilayer coverages. When coated by solid ^{4}He, however, the surface must be geometrically similar to when it is coated with solid ^{3}He. The key difference is that the exchange process between the solid and the liquid is absent in the case of ^{4}He, greatly reducing the interaction of the liquid with the surface. Indeed, Hall proposed some time ago that in these dilute mixture systems, the ^{3}He may have to tunnel through the ^{4}He barrier in order to scatter diffusely off the surface.[3]

It is also instructive to think about what constitutes a smooth substrate. Even what we would consider to be "geometrically smooth" surfaces have corrugations in the surface potential on the atomic scale. These corrugations must be smaller when the surface is coated with ^{4}He, as the potential wells in the that case are insufficiently deep to localize ^{3}He atoms.

Finally, it is important to remember that there is energy transport across the liquid-^{3}He–solid interface, so that the scattering is never completely elastic. Inelastic scattering breaks pairs regardless of the surface morphology. Another effect of ^{4}He is to cut off the inelastic channel, as is well known from the increase in thermal boundary resistance that it causes. In particular, a magnetic channel seems to couple to couple energy effectively across the interface.[79,49] We searched for a magnetic component to the boundary condition by monitoring the superfluid density (in pure ^{3}He) at constant temperature, while sweeping the magnetic field in order to change the surface polarization. No effect was visible with our resolution. However, we emphasize that the complete picture must include both momentum and energy transfer at the interface.

V. CONCLUSIONS

We have carried out a quantitative examination of the behavior of superfluid ^{3}He when confined to a film of thickness comparable to the correlation length of the order parameter. The central conclusions are as follows.

(i) Our results for pure ^{3}He exhibit generally good agreement with the Ginzburg-Landau theory, assuming that the order parameter vanishes at the surfaces.

(ii) The superfluid response is nearly bulklike when the surfaces are coated with five monolayers of ^{4}He, indicating that the quasiparticle reflections are specular, or mirrorlike.

There also remain a number of unresolved issues, which do not, however, detract from the major points. (i) We have not, despite expectation, observed the A-B phase boundary. For the moment, we assume that this is due to supercooling of the A phase. Our data overlap regions of parameter space pointed to by, for example, the calculations of Hara and Nagai and of Li and Ho. (ii) A quantitative description is lacking for the ^{3}He superfluid behavior at surfaces modified by small (nonsuperfluid) amounts of ^{4}He. For example, the superfluid ^{3}He data for our "intermediate" surface ^{4}He coverages does not mimic a Ginzburg-Landau film of some other thickness. It appears almost as if there is a temperature-independent ρ_s deficit. A more detailed understanding of the boundary conditions is needed to explain this.

ACKNOWLEDGMENTS

We gratefully acknowledge the contributions of R. S. Germain, E. Houseman, J. K. J. Lambert, D. F. McQueeney, L. Opsahl, and E. N. Smith to this work. We have enjoyed fruitful discussions and communications with A. L. Fetter, T. J. Gramila, J. P. Harrison, T.-L. Ho, J. M. Parpia, J. D. Reppy, E. V. Thuneberg, and S. Ullah. We thank the National Science Foundation (NSF) for support through Grant No. DMR-8418605, and the Cornell Material Science Center for support through NSF Grant No. DMR-8818558. M.R.F. greatly appreciates financial assistance from the Natural Science and Engineering Research Council (Canada) and the Alberta Heritage Fund.

*Permanent address: IBM Thomas J. Watson Research Center, Yorktown Heights, NY 10598.

[1]M. R. Freeman, R. S. Germain, L. Opsahl, E. Houseman, and R. C. Richardson, Jpn. J. Appl. Phys. Suppl. **26-3**, 121 (1987).

[2]M. R. Freeman, R. S. Germain, E. V. Thuneberg, and R. C. Richardson, Phys. Rev. Lett. **60**, 596 (1988).

[3]H. E. Hall, in *Liquid and Solid Helium,* edited by C. G. Kuper *et al.* (Wiley, New York, 1975).

[4]M. R. Freeman, Ph.D. thesis, Cornell University, 1988.

[5]V. L. Ginzburg and L. D. Landau, Zh. Eksp. Teor. Fiz. **20**, 1064 (1950).

[6]J. C. Wheatley, Rev. Mod. Phys. **47**, 415 (1975).

[7]N. D. Mermin and G. Stare, Phys. Rev. Lett. **30**, 1135 (1973).

[8]P. W. Anderson and W. F. Brinkman, Phys. Rev. Lett. **30**, 1108 (1973).

[9]G. Stare, Ph.D. thesis, Cornell University, 1974.

[10]V. Ambegaokar and N. D. Mermin, in *Proceedings of the 24th Nobel Symposium* (Academic, New York, 1974), p. 97.
[11]V. Ambegaokar, P. G. de Gennes, and D. Rainer, Phys. Rev. A **9**, 2676 (1974).
[12]L. J. Buchholtz and A. L. Fetter, Phys. Rev. B **15**, 5225 (1977).
[13]D. S. Greywall, Phys. Rev. B **33**, 7520 (1986).
[14]P. W. Anderson, J. Phys. Chem. Solids **11**, 26 (1959).
[15]G. Barton and M. A. Moore, J. Low Temp. Phys. **21**, 489 (1975).
[16]I. A. Privorotskii, Phys. Rev. B **12**, 4825 (1975).
[17]Y. Kuroda and A. D. S. Nagi, Physica **85B**, 131 (1977).
[18]T. Fujita, M. Nakahara, T. Ohmi, and T. Tsuneto, Prog. Theor. Phys. **64**, 396 (1980).
[19]L. H. Kjäldman, J. Kurkijärvi, and D. Rainer, J. Low Temp. Phys. **33**, 577 (1978).
[20]A. L. Fetter and S. Ullah, J. Low Temp. Phys. **70**, 515 (1988).
[21]Y.-H. Li and T.-L. Ho, Phys. Rev. B **38**, 2362 (1988).
[22]E. V. Thuneberg, Phys. Rev. B **33**, 5124 (1986).
[23]E. V. Thuneberg, Phys. Rev. B **36**, 3583 (1987).
[24]W. Zhang, J. Kurkijärvi, and E. V. Thuneberg, Phys. Rev. B **36**, 1987 (1987).
[25]L. J. Buchholtz, Phys. Rev. B **33**, 1579 (1986).
[26]J. Hara and K. Nagai (unpublished).
[27]V. L. Ginzburg and L. P. Pitaevskii, Zh. Eksp. Teor. Fiz. **34**, 1240 (1958) [Sov. Phys.—JETP **7**, 858 (1958)].
[28]L. V. Kiknadze and Yu. G. Mamaladze, Fiz. Nizk. Temp. **1** 219 (1975) [Sov. J. Low Temp. Phys. **1**, 106 (1975)].
[29]M. T. Manninen and J. P. Pekola, Phys. Rev. Lett. **48**, 812 (1982).
[30]V. Kotsubo, K. D. Hahn, and J. M. Parpia, Phys. Rev. Lett. **58**, 804 (1987).
[31]J. P. Pekola, J. C. Davis, and R. E. Packard, Jpn. J. Appl. Phys. **26-3**, 113 (1987).
[32]J. G. Daunt, R. F. Harris-Lowe, J. P. Harrison, A. Sachrajda, S. Steel, R. R. Turkington, and P. Zawadski, J. Low Temp. Phys. **70**, 547 (1988).
[33]J. C. Davis, A. Amar, J. P. Pekola, and R. E. Packard, Phys. Rev. Lett. **60**, 302 (1988).
[34]J. Harrison (private communication).
[35]K. Ichikawa, S. Yamasaki, H. Akimoto, T. Kodama, T. Shigi, and H. Kojima, Phys. Rev. Lett. **58**, 1949 (1987).
[36]V. Kotsubo, J. Ditusa, T. Hall, R. Mihailovich, and J. M. Parpia, Jpn. J. Appl. Phys. **26-3**, 143 (1987).
[37]A. J. Leggett, Ann. Phys. (N.Y.) **85**, 11 (1974).
[38]A. I. Ahonen, M. T. Haikala, and M. Krusius, Phys. Lett. **47A**, 215 (1974).
[39]Dupont Polymer Products Division, Wilmington, DE.
[40]Duke Scientific Corp., Palo Alto, CA.
[41]P. W. Adams and W. I. Glaberson, Phys. Phys. B **35**, 4633 (1987).
[42]J. D. Reppy (unpublished).
[43]Emerson and Cumming Corp., Canton, MA.
[44]W. P. Halperin, F. B. Rasmussen, C. N. Archie, and R. C. Richardson, J. Low Temp. Phys. **31**, 617 (1978).
[45]American Magnetics Corp., Oak Ridge, TN.
[46]A. I. Ahonen, M. Krusius, and M. A. Paalanen, J. Low Temp. Phys. **25**, 421 (1976).
[47]T. J. Gramila, Ph.D. thesis, Cornell University, 1989.
[48]A. I. Ahonen, T. Kodama, M. Krusius, M. A. Paalanen, R. C. Richardson, W. Schoepe, and Y. Takano, J. Phys. C **9**, 1665 (1976).
[49]P. C. Hammel, Ph.D. thesis, Cornell University, 1983.
[50]H. Godfrin, R. R. Ruel, and D. D. Osheroff, Phys. Rev. Lett. **60**, 305 (1988).
[51]H. Ramm, P. Pedroni, J. R. Thompson, and H. Meyer, J. Low Temp. Phys. **2**, 539 (1970).
[52]H. Godfrin, G. Frossati, D. Thoulouze, M. Chapellier, and W. G. Clark, J. Phys. (Paris) Colloq. **39**, C6-287 (1978).
[53]A. Schuhl, S. Maegawa, M. W. Meisel, and M. Chapellier, Phys. Rev. B **36**, 6811 (1987).
[54]Y. Okuda, A. J. Ikushima, and H. Kojima, Phys. Rev. Lett. **54**, 130 (1985).
[55]H. M. Bozler, M. E. R. Bernier, W. J. Gully, R. C. Richardson, and D. M. Lee, Phys. Rev. Lett. **32**, 875 (1974).
[56]J. D. Jackson, *Classical Electromagnetism* (Wiley, New York, 1975).
[57]H. M. Bozler, D. M. Bate, and A. L. Thomson, Phys. Rev. B **27**, 6992 (1983).
[58]E. L. Hahn and D. E. Maxwell, Phys. Rev. **88**, 1070 (1952).
[59]A. J. Leggett, Rev. Mod. Phys. **47**, 331 (1975).
[60]S. Takagi, J. Phys. C **8**, 1507 (1975).
[61]A. J. Leggett, Ann. Phys. (N.Y.) **85**, 11 (1974).
[62]D. D. Osheroff and L. R. Corruccini, Phys. Lett. **51A**, 447 (1975); W. F. Brinkman and H. Smith, *ibid.* **51A**, 449 (1975).
[63]D. N. Paulson, H. Kojima, and J. C. Wheatley, Phys. Rev. Lett. **32**, 1098 (1974).
[64]R. F. Berg, B. N. Engel, and G. G. Ihas, in *Proceedings of the 17th International Conference on Low Temperature Physics* (North-Holland, Amsterdam, 1984).
[65]P. J. Hakonen (unpublished).
[66]J. Wilks, *The Properties of Liquid and Solid Helium* (Oxford University Press, Oxford, 1967).
[67]T. J. Gramila (private communication).
[68]T. C. Padmore and J. D. Reppy, Phys. Rev. Lett. **33**, 1410 (1974).
[69]A. L. Fetter (private communication).
[70]D. Einzel, J. Low Temp. Phys. **54**, 427 (1984).
[71]J. E. Berthold, R. W. Giannetta, E. N. Smith, and J. D. Reppy, Phys. Rev. Lett. **37**, 1138 (1976).
[72]J. M. Parpia, D. G. Wildes, J. Saunders, E. K. Zeise, J. D. Reppy, and R. C. Richardson, J. Low Temp. Phys. **61**, 337 (1985).
[73]E. V. Thuneberg (private communication).
[74]J. R. G. Keyston and J. P. Laheurte, Phys. Lett. **24A**, 132 (1967).
[75]D. A. Ritchie, J. Saunders, and D. F. Brewer, Phys. Rev. Lett. **59**, 465 (1987).
[76]W. C. Black, A. C. Mota, J. C. Wheatley, J. H. Bishop, and P. M. Brewster, J. Low Temp. Phys. **4**, 391 (1971).
[77]V. P. Peshkov, in *Proceedings of the 14th International Conference on Low Temperature Physics, Helsinki, 1975,* edited by M. Krusius and M. Vuorio (North-Holland, Amsterdam, 1975), Vol. 1, p. 356.
[78]D. J. Bishop and J. D. Reppy, Phys. Rev. B **22**, 5171 (1980).
[79]L. J. Friedman, Ph.D. thesis, Cornell University, 1982.
[80]D. F. McQueeney, G. Agnolet, and J. D. Reppy, Phys. Rev. Lett. **52**, 1325 (1984).
[81]G. Agnolet, Ph.D. thesis, Cornell University, 1983.
[82]B. R. Johnson, Ph.D. thesis, Cornell University, 1984.

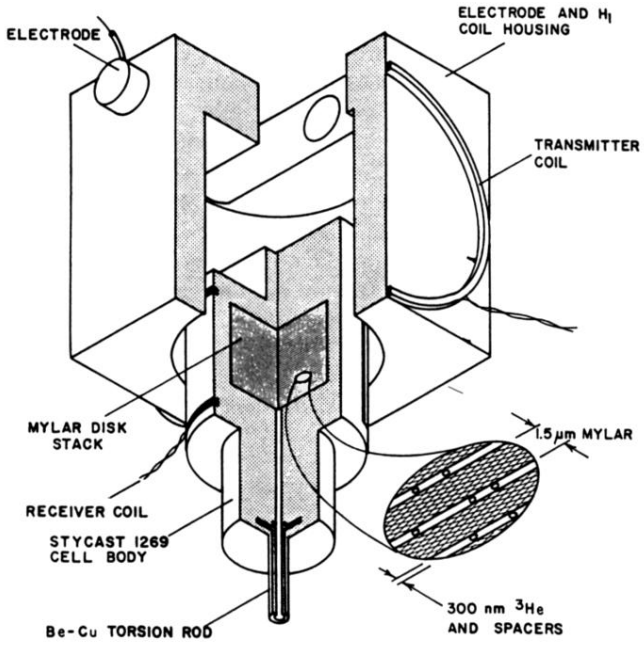

FIG. 3. The combined torsion pendulum/NMR probe. The ^{3}He in the head of the oscillator fills and cools through the hole in the torsion rod, which terminates in a small heat exchanger linked to the nuclear refrigerant. The electrode structure is thermally sunk to the mixing chamber.